Electronic Supplementary Material (ESI) for Physical Chemistry Chemical Physics.

Supplementary information

Enhancing overall properties of epoxy-based composites using polydopamine coated edge-carboxylated graphene prepared via one-step high pressure ball-milling

Shujie Ren [a], Liu Meng [a], Wenli Ma [a], Song Lin [c], Wengang Yang [a], Jinle Lan [a], Xiaolong Jia [a,b,*], Qing Cai [a], Xiaoping Yang [a,b]

[a]State Key Laboratory of Organic-Inorganic Composites, College of Materials Science and Engineering, Beijing University of Chemical Technology, Beijing 100029, P. R. China,

[b]Key Laboratory of Carbon Fiber and Functional Polymer, Ministry of Education, Beijing University of Chemical Technology, Beijing 100029, P. R. China

[c]North China Institute of Aerospace Engineering, Hebei 065000, P. R. China

*Corresponding author

E-mail: jiaxl@mail.buct.edu.cn; Tel/Fax: +86-10-6442-7698.

TFBT samples were prepared as presented in Fig. S1 in reference to our previous works.[1-2] A bundle of CF was placed in the middle narrow slit of the mold and kept under tension. After the degassed EP mixture containing various contents of p-ECG was slowly poured into the mold, the final TFBT samples were obtained by curing at 80 °C /1 h + 120 °C /2 h + 150 °C /3 h.

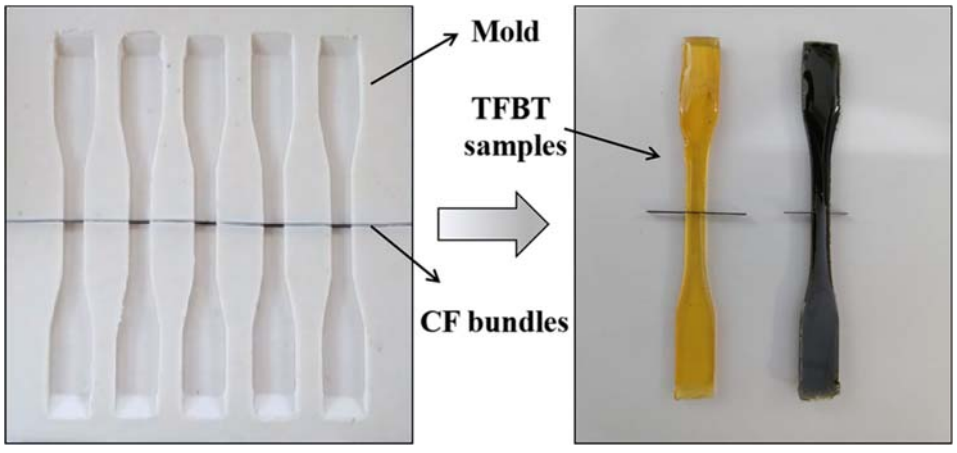

Fig. S1 Schematic graphs of the used mold and the obtained TFBT samples.

The prepared p-ECG was characterized by FTIR, XPS and TGA. As shown in the FTIR spectra (Fig. S2), the characteristic aromatic C=C stretching band of graphite was clearly observed at 1624 cm^{-1}. For the FTIR spectrum of ECG, an additional absorption peak appeared at 1717 cm^{-1}, which should be originated from the C=O stretching in the carboxyl group functionalized at the edge of graphite. Compared to the FTIR spectrum of ECG, the peak at 1717 cm^{-1} disappeared, while two new absorption peaks appeared at 1610 and 1028 cm^{-1} in the spectrum of p-ECG. These two new peaks were corresponded to the N-H bending vibration and the C-OH stretching vibration from pDop.[3] These facts suggested the successful incorporation of pDop component onto ECG sheets.

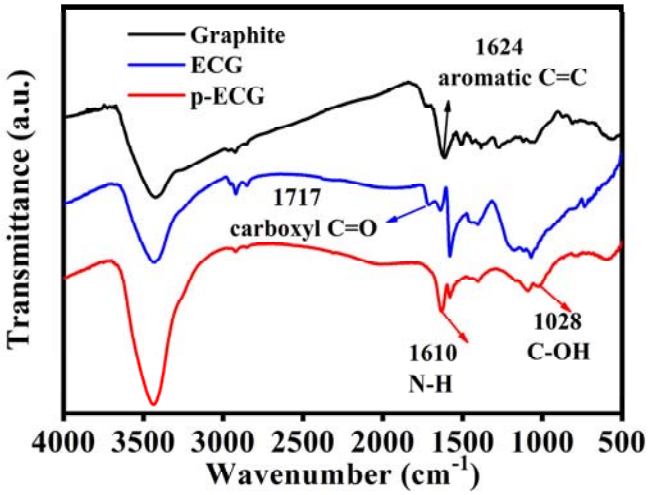

Fig. S2 FTIR spectra of graphite, ECG and p-ECG.

Surface compositions of p-ECG were then identified by XPS analysis. Fig. S3 shows XPS spectra of graphite, ECG and p-ECG, and Table S1 lists the atom content of each corresponding element. In Fig. S3(a), both graphite and ECG displayed C_{1s} signal at 284.6 eV and O_{1s} signal at 533.2 eV, which were assigned to the graphitic carbons and oxygen-containing groups, respectively. And the oxygen atom content in ECG was 22.4 %, higher than the value of 8.8 % in graphite, indicating the successful introduction of carboxyl-type groups onto graphite using dry ice as the reaction source through ball-milling. In addition to the above two signals, an extra N_{1s} signal at 401.0 eV was observed in p-ECG, which was definitely attributed to the nitrogen atom in dopamine. Deconvolution of the C_{1s} peak in p-ECG demonstrated two kinds of signals at 284.7 and 289.8 eV, corresponding to sp2 and sp3 hybridized carbon of graphite structure and O-C=O of carboxyl group, respectively (Fig. S3(b)). Besides, the O/C atomic ratio of p-ECG was calculated to be 0.4, which was higher than that (0.3) of ECG (Table S1). These data revealed the presence of pDop component in p-ECG. In Fig. S3(c), the N_{1s} peaks of p-ECG appearing at 401.7, 399.8 and 398.5 eV, originated

from the -N=, -NH- and -NH_2 structure, respectively, which was highly consistent with the polymerization mechanism of dopamine proposed by Hong S et al.[4] In addition, some of the secondary amine might come from the reaction on GN between amino group of dopamine and oxygen groups (eg, epoxide group) generated from dry ice through ball-milling. In considering both the FTIR and XPS data, thus, the preparation of pDop modified GN was confirmed.

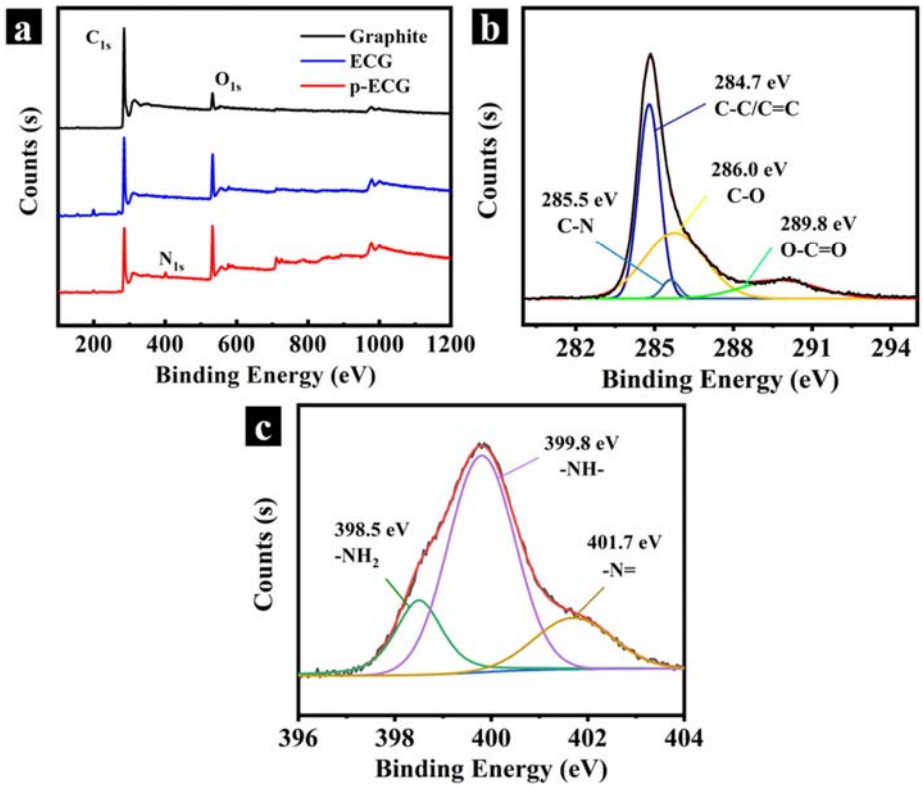

Fig. S3 (a) Survey XPS spectra of graphite, ECG and p-ECG, (b) C_{1s} for p-ECG and (c) N_{1s} for p-ECG.

Table S1 Atom content (%) of each element in graphite, ECG and p-ECG through XPS analysis

Sample	C_{1s}	O_{1s}	N_{1s}	O/C
Graphite	91.2	8.8	0	0.1
ECG	77.6	22.4	0	0.3
p-ECG	68.4	27.7	3.9	0.4

Raman spectroscopy was a common characterization method for evaluating micro-structure of graphene by the ratio between the relative intensities of the D band to the G band (I_D/I_G). Fig. S4 shows the Raman spectra of graphite, ECG and p-ECG. All samples showed D and G bands at the ranges of 1328-1345 and 1560-1600 cm^{-1}, respectively, reflecting the disorder and symmetry of the graphene sheets.[5] It was found that the intensity of the D band of graphite was weak, and the I_D/I_G value was as low as 0.08. This was because the graphite flake size was large with small amount of structural defects. After the ball-milling, the I_D/I_G value for the obtained ECG significantly increased to be about 1.06, indicating that the graphite flake size was much reduced along with obvious structural change resulted from edge-carboxylated functionalization. For the final sample p-ECG, the I_D/I_G value further increased to be about 1.25, which proved that the reduction and coating on the obtained ECG were readily achieved via the mild oxidative polymerization of mussel-inspired dopamine. In addition, the G band position of p-ECG moved toward the high frequency with respect to ECG and graphite, which also indicated that the graphite sheet layer was peeled off to be thinner under the function of ball-milling and the intercalation of polydopamine.

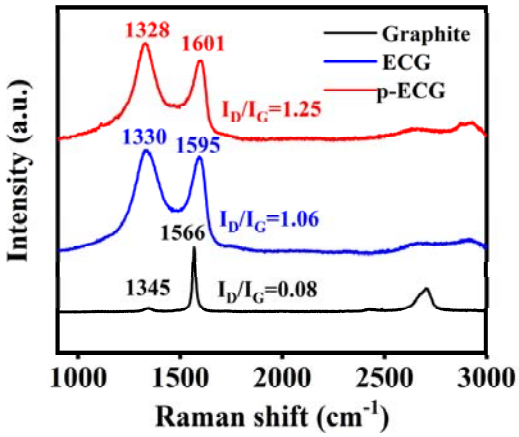

Fig. S4 Raman spectra of graphite, ECG and p-ECG.

TGA measurements were conducted to evaluate the effect of pDop on the thermal stability of p-ECG. As shown in Fig. S5, a small weight loss of 2.4 wt.% was finally found for graphite because of the decomposition of oxygen-functional groups in graphite. Different from graphite, a rapid weight loss of ECG started around 180 °C, indicating a large amount of oxygen-functional groups decomposed above this temperature.[6] The final weight residue of ECG leveled off at ~66 wt.%. In the case of pDop, the main decomposition occurred at temperature above 200 °C, which

was attributed to the quick loss of active groups like -OH and -NH_2 containing in pDop. Noticeably, p-ECG also started a rapid weight loss at the temperature of ~180 °C, and the leveled weight loss was ~38 wt.%, indicating its high carbon residue quantity upon heating in N_2 atmosphere. In comparison with both ECG and pDop, the weight loss of p-ECG was unexpected to be at a lower value, suggesting the higher thermal stability. This enhancement in thermal stability was supposed as a result of the amide-like structure formed onto p-ECG by the chemical reaction between the generated carboxyl group and amine group in pDop through ball-milling. Moreover, the grafted weight fractions of carboxyl group and pDop could be calculated from TGA data using the equations of $\left(1\text{-}f_{graphite}\right)Y = f_{ECG} - f_{graphite}$ and $Xf_{pDop} + \left(1-X\right) f_{graphite} = f_{p\text{-}ECG}$, respectively, where $f_{graphite}$, f_{ECG} and $f_{p\text{-}ECG}$ are the weight loss fraction of graphite, ECG and p-ECG, accordingly, as well as Y and X denote the weight fraction of carboxyl-type group in ECG and pDop in p-ECG. The calculated weight fractions of carboxyl-type group in ECG and pDop in p-ECG were ~32 and 55 wt.%, respectively.

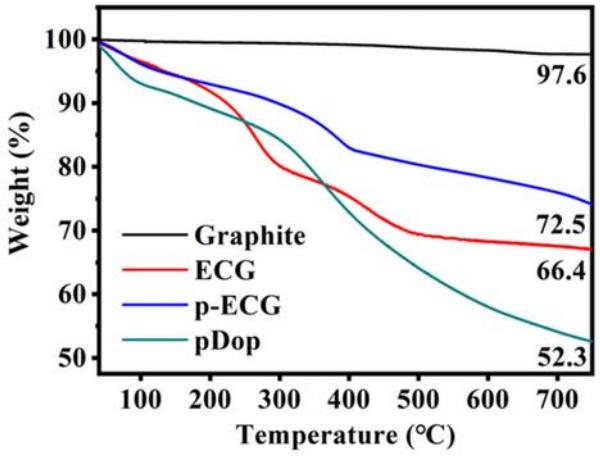

Fig. S5 TGA curves of graphite, p-ECG, ECG and pDop.

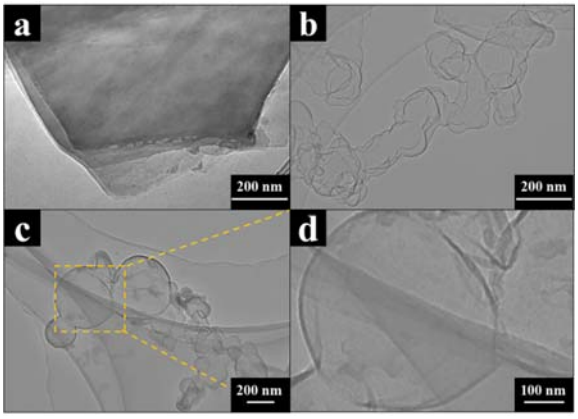

Fig. S6 TEM images of samples prepared using ball-milling under different pressures of (a) 5, (b) 8 and (c) 11.5 MPa at the temperature of 60 ℃. The graph in panel (d) is the high-magnification image of the selected area in panel (c).

The effect of the pressure during the ball-milling on the structure and morphology of the resulted products was evaluated systematically. Here, the products prepared at 60 °C were selected as the typical examples. As shown in Fig. S6(a), when the pressure was as low as 5.0 MPa, the resulted sample was not stripped well, showing irregular shapes with sharp edges similar to the morphology of the graphite powders. With the pressure ascending, the sample having thin thickness and smooth edges gradually obtained along with the proportion of round shape GN in the product increasing (Fig. S6(b)). When the pressure reached as high as 11.5 MPa, the sample with special round shape and small sheet size was fabricated (Fig. S6(c,d)).

The dispersion state of p-ECG in EP matrix is presented in OM images of Fig. S7. As shown in Fig. S7(a-c), most of p-ECG sheets were scattered in the EP matrix evenly with sporadic aggregations when the content of p-ECG was in a low value range. However, the amount of p-ECG aggregates would increase as the content of p-ECG in EP composites increasing. This was commonly observed in research works relating to nanofillers.[7-9] As shown in Fig. S7(d), p-ECG aggregates had been so obvious that their adverse effect on mechanical properties of composites could not be ignored. The structural defects resulted from the insufficient impregnation of EP resin into p-ECG aggregates would generate stress concentration during mechanical property evaluation, thus led to the subsequent decrease in mechanical strength and modulus.

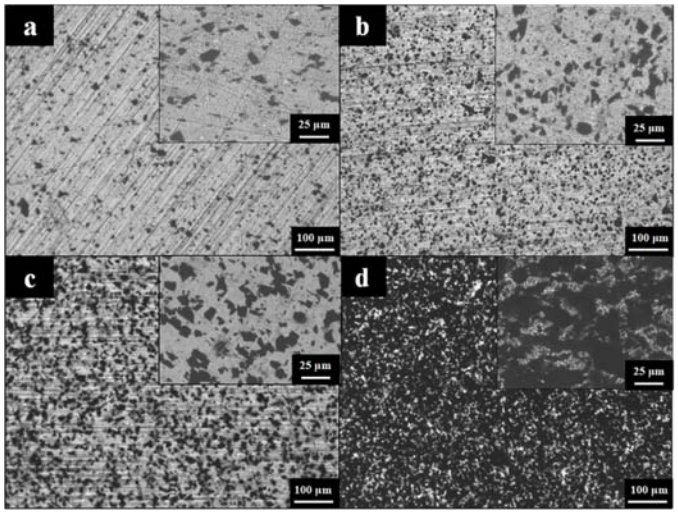

Fig. S7 OM images of EP composites with (a) 0.1, (b) 0.2, (c) 0.5 and (d) 1.0 wt.% p-ECG. The insets are the high-magnification images.

p-ECG had demonstrated effective reinforcing effect on EP composites by combining the inherent adhesive feature of dopamine and the interfacial amine-EP reaction. Fig. S8 showed the schematic for the chemical reaction at the interfacial area between p-ECG and EP matrix. The primary and secondary amine groups on p-ECG could be reactive with epoxide group of EP matrix. p-ECG showed the capacity to enhance the curing process of EP resin. The reactions between p-ECG and EP resin enabled p-ECG being involved into the crosslinked structure of EP matrix during thermal curing, which led to a strong interfacial bonding.

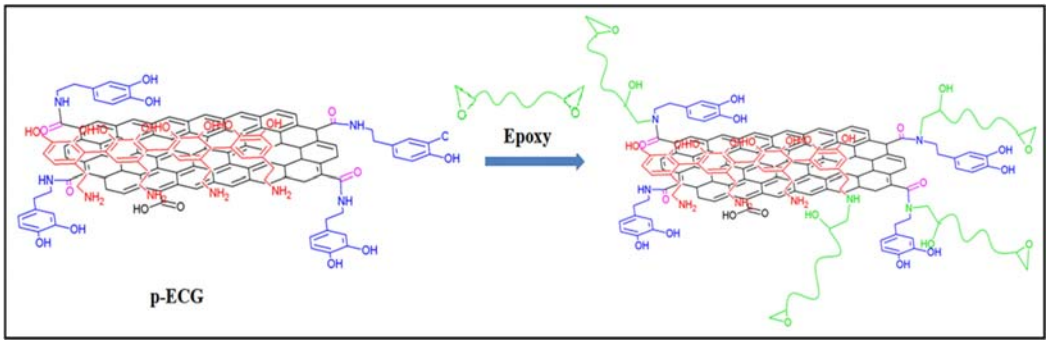

Fig. S8 Schematic for the chemical reaction at the interfacial area between p-ECG and EP matrix.

Fig. S9 showed the EDS results for marked rectangle regions in Fig. 8(f). It was found that three marked regions were mainly composed of C, N and O elements. The atom content of each element in region A was different from that in region B or region C. The O/C atomic ratio in region A was calculated to be around 0.45 (Fig. S9(a)), which was close to the O/C atomic ratio value for p-ECG calculated using XPS data in Table S1. Since region A was selected from the distributed nanoparticles, the EDS result proved that these nanoparticles on the surface of CF were p-ECG nanofillers. Among these three regions, the highest atom content of C element was detected in region B (Fig. S9(b)), which was the typical feature of CF. This confirmed that region B belonged to CF. Region C located at the EP matrix area between CFs. Compared with region A and region B, region C contained higher atom content of N element (Fig. S9(c)). The additional N element in region C definitely came from the amine curing agent in EP matrix.

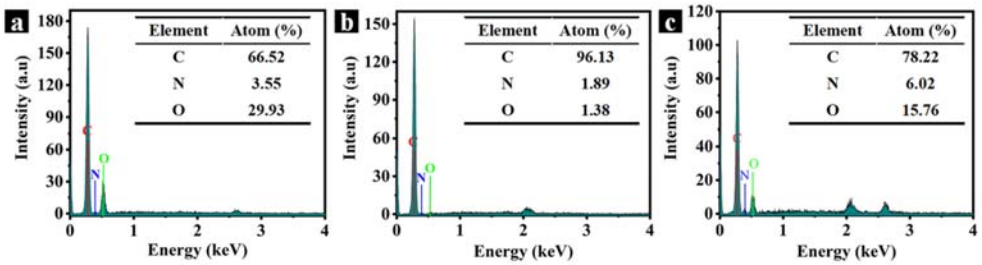

Fig. S9 EDS results for marked rectangle regions of (a) A, (b) B and (C) in Fig. 8(f).

The electrical conductivities of various CFs and CF/EP composites are listed in Table S2. It was found that the electrical conductivity was 709.2 S/cm for desized CF, much higher than 478.5 S/cm for commercial CF, indicating that the existence of sizing agent negatively affected the electrical performance of CF. This was because the sizing agent was mainly composed of EP, which was a kind of electrical insulating material. Compared to the desized CF, the value for p-ECG@desized CF increased by 22.6 % and reached 869.6 S/cm. As expected, in comparison with desized CF and p-ECG@desized CF, the electrical conductivity values decreased for both desized CF/EP and p-ECG@desized CF/EP composites after combining with EP due to electrical insulating characteristics of EP. However, it was worth noting that p-ECG@desized CF/EP composites showed an 19.7 % enhancement in electrical conductivity compared with desized CF/EP composites.

Table S2 Electrical properties of various CFs and CF/EP composites

	Electrical conductivity (S/cm)	Electrical resistivity (μΩ·cm)
commercial CF	478.5	2.09
desized CF	709.2	1.41
p-ECG@desized CF	869.6	1.15
desized CF/EP	186.9	5.35
p-ECG@desized CF/EP	223.7	4.47

References

[1] M. He, P. Qi, P. Xu, Q. Cai, P. Li, X. Jia and X. Yang, *Compos. Sci. Technol.,* 2019, **173,** 24-32.

[2] P. Xu, Y. Yu, Z. Guo, X. Zhang, G. Li and X. Yang, *Compos. Sci. Technol.,* 2019, **171,** 252-260.

[3] T. An, N. Lee, H. J. Cho, S. Kim and S. M. Lee, *RSC Adv.*, 2017, **7**, 30582-30587.

[4] S. Hong, S. N. Yun, S. Choi, I. T. Song and H. Lee, *Adv. Funct. Mater.*, 2012, **22**, 4711-4717.

[5] Z. Jian, L. Zhensheng, L. Hongqi, H. Wenbin, Z. Changzhi, Z. Peng and S. Donglu, *Langmuir,* 2015, **31,** 2576-2583.

[6] B. Dehghanzad, M. K. R. Aghjeh, O. Rafeie, A. Tavakoli and A. J. Oskooie, *Rsc Adv.*, 2016, **6**, 3578-3585.

[7] M. Farmahini-Farahani, H. Xiao and Y. Zhao, *J. Appl. Polym. Sci.*, 2014, **131**, 1366-1373.

[8] W. Zheng, W. G. Chen, Q. Zhao, S. X. Ren, Y. Q. Fu, *Polymer,* 2019, **163,** 171-177.

[9] A. K. Pathak, M. Borah, A. Gupta, T. Yokozeki and S. R. Dhakate, *Compos. Sci. Technol.*, 2016, **135**, 28-38.